



## Electrochemical Characterization of Charge Injection at Electrodeposited Platinum Electrodes in Phosphate Buffered Saline

John J. Whalen III,<sup>a</sup> Jeffrey Young,<sup>a</sup> James D. Weiland,<sup>a</sup> and Peter C. Searson<sup>b,\*</sup>

<sup>a</sup>Doheny Vision Research Center, University of Southern California, Los Angeles, California 90033, USA

<sup>b</sup>Department of Materials Science and Engineering, Johns Hopkins University, Baltimore, Maryland 21218, USA

Platinum exhibits biocompatibility and chemical stability over a wide potential range and hence is a candidate material for implantable electrodes. Electrodeposition is of interest for the fabrication of implantable electrodes since it is compatible with a wide range of patterning techniques, including conventional microfabrication, soft-lithography, and electrochemical template synthesis. We show that surface roughness of platinum electrodes deposited from ammonium hexachloroplatinate solution is dependent on the deposition potential. We demonstrate that 600  $\mu\text{m}$  diameter electrodeposited platinum microelectrodes can inject 200 nC of charge in a 2 ms biphasic pulse with a potential window as small as 200 mV.  
© 2006 The Electrochemical Society. [DOI: 10.1149/1.2354457] All rights reserved.

Manuscript submitted March 17, 2006; revised manuscript received July 5, 2006. Available electronically October 11, 2006.

Stimulatory electrodes are used in a wide range of applications including deep brain and cochlear implants, retinal and cortical prostheses, stimulation of the bladder and spinal cord, and cardiac pacing.<sup>1,2</sup> The electrical stimulation of cells requires the injection of charge. In this type of biomedical application, a balanced-charge biphasic waveform is generally used to prevent tissue damage induced by irreversible electrochemical reactions occurring at the electrode/tissue interface.<sup>3</sup> The performance of noble metal stimulating electrodes is determined in large part by the charge that can be delivered within the potential limits associated with hydrogen and oxygen evolution.<sup>1,3</sup> Within these limits, charge injection can occur through double-layer charging or by reversible faradaic processes such as oxide formation and reduction, and hydrogen adsorption/desorption. Irreversible faradaic processes that result in the formation of chemical species in bulk solution can adversely affect the tissue.<sup>1-3</sup> Materials that have been studied for stimulating electrodes include platinum, iridium oxide, and titanium nitride.<sup>4-7</sup>

Platinum is widely used in implantable electrodes for both stimulation and recording since it exhibits good biocompatibility and is stable over a wide potential range. Since the double-layer capacitance is typically  $20 \mu\text{F cm}^{-2}$  and the potential window is about 1 V, the baseline capacitance available for cell stimulation by double-layer charging alone is about  $20 \mu\text{C cm}^{-2}$ . Additional charge can be obtained from the adsorption and desorption of hydrogen [ $\text{Pt} + \text{H}^+(\text{aq}) + \text{e}^- \leftrightarrow \text{Pt}-\text{H}_{\text{ads}}$ ], from oxide formation and reduction [ $\text{Pt} + \text{H}_2\text{O} \leftrightarrow \text{PtO}(\text{s}) + 2\text{H}^+ + 2\text{e}^-$ ], and from anion adsorption (e.g.,  $\text{Pt} + \text{Cl}^- \leftrightarrow \text{Pt}-\text{Cl}_{\text{ads}} + \text{e}^-$ ). These processes are reversible since the corresponding back-reaction occurs on applying a potential pulse of opposite polarity. Reactions involving the formation of gases and soluble dissolution products are irreversible, since these reaction products diffuse away from the electrode surface and cannot be completely converted back to the corresponding reactants. Although platinum can be dissolved in chloride solutions with the formation of soluble species (e.g.,  $\text{PtCl}_6^{2-}$  and  $\text{PtCl}_4^{2-}$ ), the rate of reaction is sufficiently slow that the concentration released into the surrounding tissue can be neglected, even after long periods of stimulation.<sup>3</sup>

In previous work<sup>8</sup> we have shown that platinum can be deposited from ammonium hexachloroplatinate solution at neutral pH over a potential range where hydrogen evolution can be avoided. Furthermore, we have shown that the morphology and grain size of the deposited films is dependent on the deposition potential. These features provide the opportunity to fabricate implantable electrodes

with properties that can be tailored for specific applications. In this paper we report on the electrochemical behavior of electrodeposited platinum films and microelectrodes in phosphate buffered saline. We show that the charge capacity is strongly dependent on the morphology and surface chemistry of the films.

### Experimental

Platinum was deposited from solution containing 17 mM  $(\text{NH}_4)_2\text{PtCl}_6$  (Alfa Aesar) and 250 mM  $\text{Na}_2\text{HPO}_4$  (Alfa Aesar, ACS grade) at pH 7.8. The details have been reported elsewhere.<sup>8</sup> Platinum films were deposited on polycrystalline gold films or platinum microelectrodes. Gold films ( $>200 \text{ nm}$  thick) were thermally evaporated onto Si(111) wafers with a 20 nm chromium adhesion layer. Prior to each experiment, films were immersed in acetone and rinsed sequentially in isopropanol, ethanol, and water. Finally, the films were immersed in 5 M nitric acid and rinsed in water. Platinum foils (Alfa Aesar, Premion 99.99%) were annealed in air at  $700^\circ\text{C}$  for 2 h. After annealing the films were etched in nitric acid solution and rinsed in distilled, deionized water.

Platinum films were deposited at constant potential for 2 h corresponding to deposition film thicknesses of 30–195  $\mu\text{m}$ . Films were characterized by cyclic voltammetry and impedance spectroscopy in phosphate buffered saline (Gibco Brand, Invitrogen): 0.1 M  $\text{K}_2\text{HPO}_4$ , 0.1 M  $\text{Na}_3\text{PO}_4$ , and 0.15 M NaCl (pH 7.4).

Charge injection experiments were performed on platinum disk microelectrode arrays. The arrays were comprised of 600  $\mu\text{m}$  diam ( $A = 0.00283 \text{ cm}^2$ ) disk electrodes embedded in a silicone elastomer. Prior to electrodeposition of platinum, the platinum microelectrodes were cycled at least 40 times in 250 mM  $\text{H}_2\text{SO}_4$  (pH 1.8) over the potential range from  $-0.2$  to  $1.25 \text{ V}$  (Ag/AgCl) at a scan rate of  $250 \text{ mV s}^{-1}$  to ensure reproducible surfaces. Electrodes were then rinsed in deionized water prior to electrodeposition of platinum at potentials from  $-0.4$  to  $-0.8 \text{ V}$  (Ag/AgCl) for 1 h.

Platinum microelectrodes were characterized in 250 mM  $\text{H}_2\text{SO}_4$  (pH 1.8) and in phosphate buffered saline (PBS). Charge injection experiments were performed on the microelectrodes in a two-electrode configuration using a biphasic current pulse with a duration of 1 ms.<sup>9</sup> The experiments were performed in PBS at room temperature with a platinum mesh counter electrode.

### Results and Discussion

**Platinum films.**—Figure 1 shows voltammograms for a gold electrode in supporting electrolyte and in ammonium hexachloroplatinate solution. The details have been reported elsewhere.<sup>8</sup> Briefly, the onset of platinum ion reduction occurs at  $0.2 \text{ V}$  (Ag/AgCl); however, the current in the potential range from

\* Electrochemical Society Active Member.

<sup>z</sup> E-mail: searson@jhu.edu

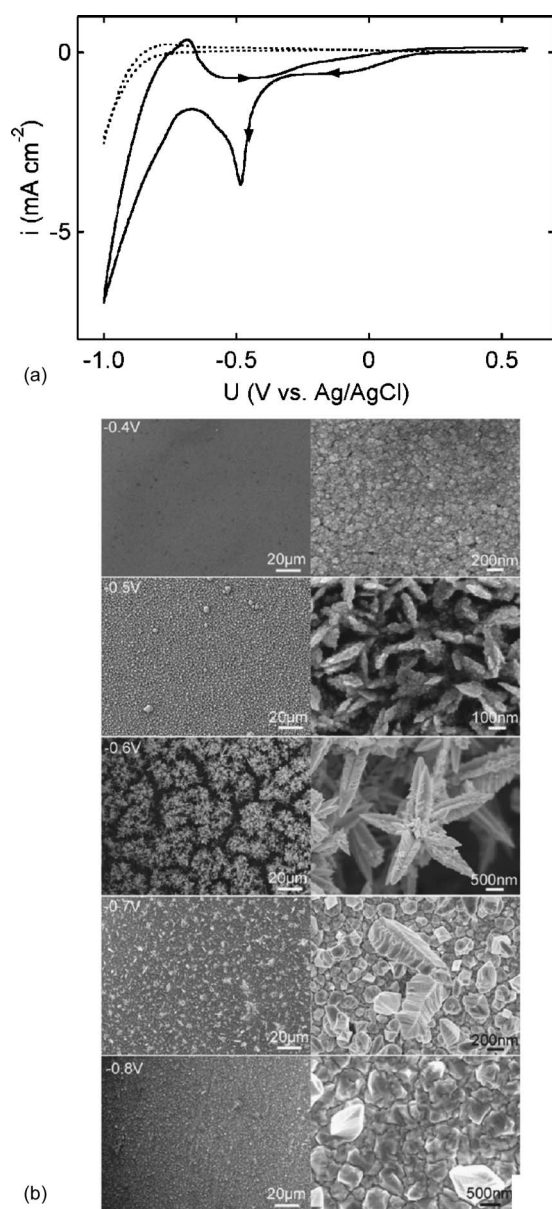


**Figure 1.** (a) Current–voltage curves for gold in supporting electrolyte (dashed line) and in ammonium hexachloroplatinate solution (solid line). The scan rate was  $50 \text{ mV s}^{-1}$ . (b) Plan-view SEM images of electrodeposited platinum films.

0.2 to  $-0.3 \text{ V}$  corresponds to the reduction of Pt(IV) to Pt(II). The onset of bulk deposition at  $-0.3 \text{ V}$  is followed by a current peak at  $-0.5 \text{ V}$  characteristic of nucleation and diffusion-controlled growth. The equilibrium potential for hydrogen evolution at this pH is  $-0.71 \text{ V}$  (Ag/AgCl), illustrating that platinum can be deposited from this solution in a potential range positive to the onset of hydrogen evolution, thereby avoiding effects associated with the co-deposition of hydrogen, such as internal stresses. This is not possible in acidic solutions where the equilibrium potential for hydrogen evolution is shifted positive by about  $450 \text{ mV}$ , close to the onset of platinum deposition.<sup>10</sup>

The morphology of platinum films deposited from this solution is strongly dependent on the deposition potential, as shown in the plan-view scanning electron microscope images in Fig. 1. Films deposited at  $-0.4 \text{ V}$  are smooth and bright. At high magnification, the films appear dense with spherical grains approximately  $10 \text{ nm}$  in diameter. At  $-0.5 \text{ V}$ , the films exhibit nodular features about  $1 \mu\text{m}$

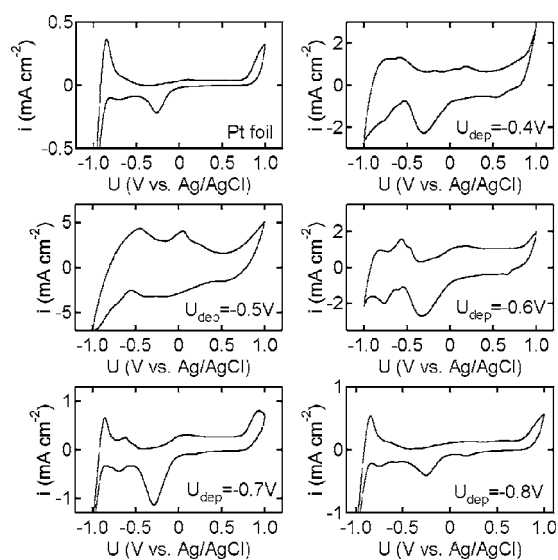


**Figure 2.** Current–voltage curves for annealed polycrystalline platinum foil and electrodeposited platinum films in PBS solution (pH 7.4). The potential range was  $-1.0$  to  $1.0 \text{ V}$  and the scan rate was  $50 \text{ mV s}^{-1}$ .

in diameter. At high magnification these features are porous, consisting of needle-like crystals up to a few hundred nanometers in length. The films deposited at  $-0.6 \text{ V}$  exhibit similar characteristics, although the features are somewhat larger. The nodular features seen at low magnification are about  $10 \mu\text{m}$  in diameter. At high magnification these features are seen to be composed of faceted, needle-like crystals up to  $1 \mu\text{m}$  in length. At  $-0.7$  and  $-0.8 \text{ V}$  the films appear smooth, bright, and dense, with grain sizes on the order of  $100 \text{ nm}$ . Although the evolution of the morphology with deposition potential is unusual, the results were highly reproducible.

Thin films formed at  $-0.5$  and  $-0.6 \text{ V}$  are of particular interest due to the high surface area. For stimulation applications, high-surface-area electrodes exhibit increased charge capacity so that lower potential limits can be used to achieve the capacities needed for depolarization with minimal contribution from faradaic reactions. High-surface-area platinum electrodes can be formed by several methods. Platinum black is usually deposited from acidic  $\text{PtCl}_6^{2-}$  solution at high current density with the addition of  $\text{Pb}(\text{NO}_3)_2$  or  $\text{Pb}(\text{CH}_3\text{COOH})_2$ .<sup>11,12</sup> For implant applications, platinum black is undesirable due to its poor mechanical stability and the incorporation of lead into the deposited film. High-surface-area electrodes can also be formed by cycling platinum in  $\text{H}_2\text{SO}_4$  at high rate for several hours.<sup>6,13</sup> During cycling, sequential oxide formation and reduction results in the formation of a porous structure with roughness factors as high as 70. The films deposited in this work can be deposited quickly, have high surface area, are relatively robust, and do not contain toxic impurities.

In previous work we have shown that with increasing deposition overpotential, the films exhibit increasing (111) texture.<sup>8</sup> At more positive potentials (200), (220), and (311) peaks are also observed. X-ray photoelectron spectroscopy has shown that the films deposited at  $-0.5$  to  $-0.8 \text{ V}$  exhibit a thin, compact  $\text{PtO}_2$  layer at the surface. The film deposited at  $-0.4 \text{ V}$ , however, has a much thicker mixed oxide of PtO and  $\text{PtO}_2$ .

In vitro characterization of implantable electrodes is usually performed in phosphate-buffered saline. Figure 2 shows voltammograms for the electrodeposited films and an annealed platinum foil in PBS. In contrast to acidic solutions, the effective potential range for charging is significantly larger at this pH due to the negative shift in the onset of hydrogen evolution and the large overpotential for oxygen evolution. The voltammogram for the annealed polycrystalline platinum foil shows the same general features as in sulfuric acid

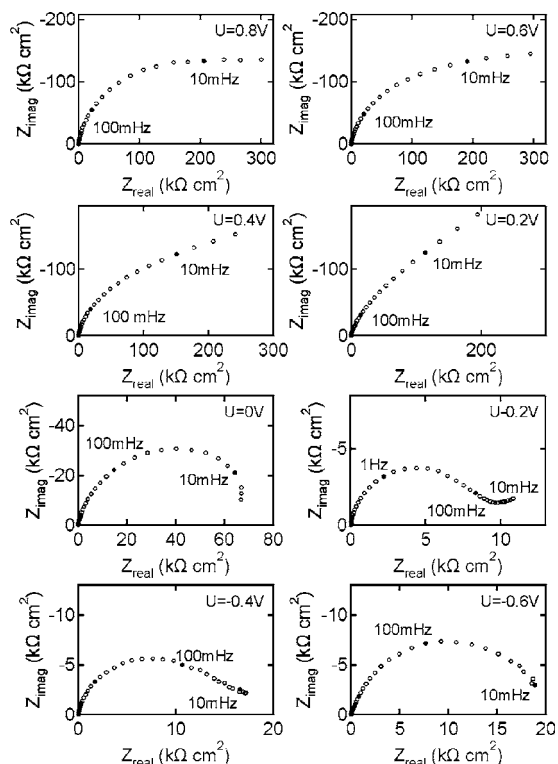


**Figure 3.** Complex plane plots for an annealed polycrystalline platinum foil in PBS. The potentials are indicated in the plots.

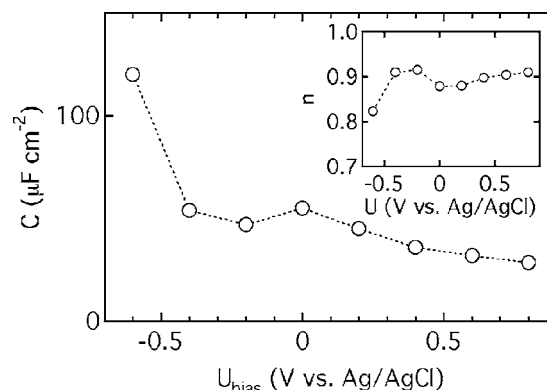
with hydrogen adsorption and desorption peaks, a double-layer charging region, an oxide formation plateau, and an oxide reduction peak.<sup>14</sup> Similar results have been reported for polished polycrystalline platinum in PBS under comparable conditions.<sup>4,15,16</sup> The film deposited at  $-0.4$  V exhibits relatively broad features and large capacitive charging, presumably related to the relatively thick mixed oxide at the surface. The high-surface-area film deposited at  $-0.5$  V exhibits large currents and broad, slightly sheared features characteristic of a non-negligible film resistance. Similar features have been reported for electrodes fabricated by electrodeposition of platinum onto high-surface-area gold with a roughness factor of about 10.<sup>17</sup> The high-surface-area films deposited at  $-0.6$  V exhibit slightly smaller currents but more distinct features. The voltammograms for the films deposited at  $-0.7$  and  $-0.8$  V are very similar to the annealed platinum foil.

The electrochemical response of the electrodeposited platinum films was also characterized using electrochemical impedance spectroscopy. Figure 3 shows complex plane plots for the annealed platinum foil in PBS in the potential range from  $-0.6$  to  $0.8$  V. The impedance response in the hydrogen and double-layer regime, from  $-0.6$  to  $0$  V, shows a characteristic semicircular loop. At  $0.2$  and  $0.4$  V, corresponding to the onset of oxide formation, the complex plane plots exhibit some dispersion at low frequencies; however, at more positive potentials,  $0.6$  and  $0.8$  V, the complex plane plots are slightly depressed semicircular loops.

The semicircular loop is associated with charge transfer at the interface and was modeled using an equivalent circuit with a resistance,  $R_s$ , in series with a resistance,  $R_p$ , in parallel with a constant phase element, CPE. The total impedance of the equivalent circuit is

$$Z(\omega) = \frac{R_s + R_p + R_s R_p Q (i\omega)^n}{1 + R_p Q (i\omega)^n} \quad [1]$$

where the CPE is represented by an equivalent capacitance,  $Q$ , and an exponent,  $n$ .<sup>18</sup> In most cases, fitting produced  $n > 0.9$ , and we take  $Q = C$ .



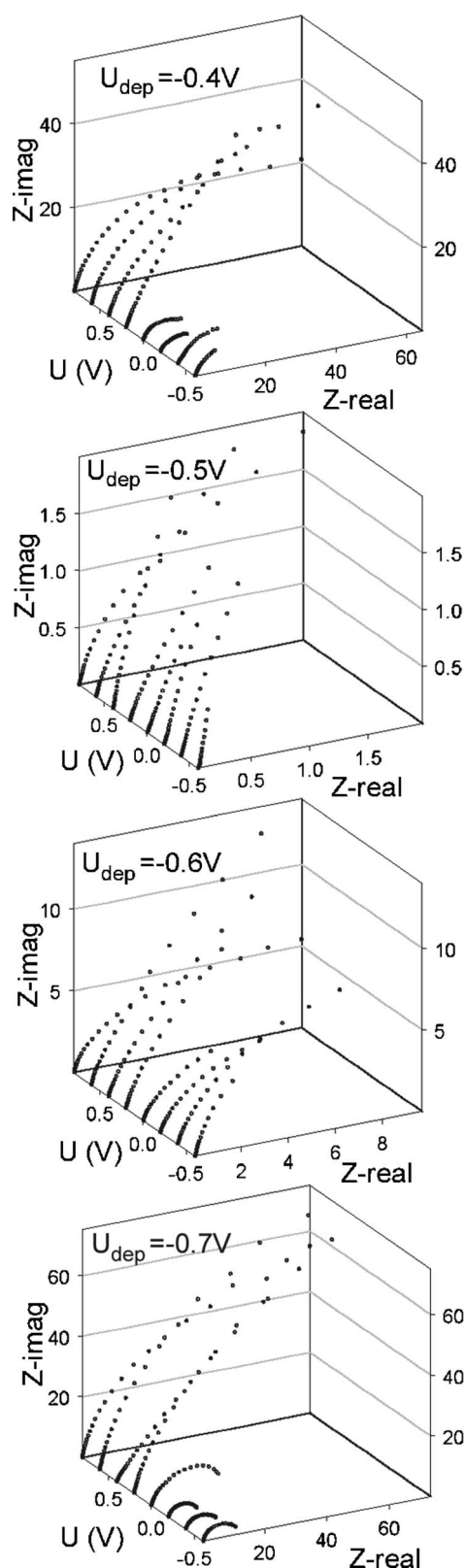
**Figure 4.** Parallel capacitance vs potential for an annealed polycrystalline platinum foil in PBS. The inset shows the dependence of the exponent  $n$  on potential.

Figure 4 shows the total capacitance  $C$  and exponent  $n$  vs potential for the annealed platinum film. The capacitance decreases from about  $120 \mu\text{F cm}^{-2}$  at  $-0.6$  V, in the hydrogen regime, to about  $30 \mu\text{F cm}^{-2}$  at  $0.8$  V, in the oxide regime. The exponent  $n$  was greater than  $0.9$  over most of the potential range. Similar curves have been reported for the total capacitance of platinum in acidic sulfate and acidic chloride solutions.<sup>19,20</sup> As described above, the capacitance is somewhat larger than typical double-layer capacitances due to the additional contribution from reversible ion adsorption ( $\text{H}^+$ ,  $\text{Cl}^-$ , and  $\text{OH}^-$ ) over the whole potential range.

Figure 5 shows complex plane plots of the impedance response of the electrodeposited platinum films in PBS over the potential range from  $-0.6$  to  $0.8$  V. The complex plane plots for the film deposited at  $-0.4$  V are similar to those for the platinum foil. At potentials from  $-0.6$  to  $0$  V, a single semicircular loop is seen. At  $0.2$  and  $0.4$  V the loop is much larger, indicating a large increase in the parallel resistance, and also exhibits some dispersion at lower frequencies. At more positive potentials, at  $0.6$  and  $0.8$  V, the parallel resistance decreases resulting in a slightly smaller loop. The complex plane plots for films deposited at  $-0.5$  and  $-0.6$  V are much more capacitive, as expected from the high surface area. The complex plane plots for the film deposited at  $-0.7$  V are similar to those for the annealed platinum foil.

The total capacitance and exponent of the electrodeposited films are plotted vs potential in Fig. 6a. As for the case of the annealed foil, the capacitance of the electrodeposited films decreases with increasing potential. However, the magnitude of the capacitance spans more than two orders of magnitude. The exponents for the films deposited at  $-0.6$  and  $-0.7$  V are close to  $0.9$  over most of the potential range, as seen in Fig. 6b, consistent with the results on the annealed platinum foil. The lower exponents associated with the films deposited at  $-0.4$  V may be related to the surface chemistry. As described above, the films deposited at  $-0.4$  V exhibit mixed Pt(III)/Pt(IV) oxide rather than the thin  $\text{PtO}_2$  film seen at more negative deposition potentials. Figure 6c shows the capacitance obtained from the impedance spectra at  $0.4$  V plotted vs the surface roughness. The surface roughness was determined from the hydrogen desorption charge in voltammograms in  $\text{H}_2\text{SO}_4$ .<sup>8</sup> The linear dependence with a slope of one shows that the electrode capacitance is directly related to the surface roughness. These results also demonstrate that the differences in capacitance associated with the different films are related only to the differences in surface area and not due to differences in surface chemistry.

**Platinum microelectrodes.**— Since stimulation and recording applications require microelectrodes, we have characterized the performance of electrodeposited platinum microelectrodes. Figure 7 shows voltammograms for platinum microelectrodes in  $250 \text{ mM H}_2\text{SO}_4$ . The voltammogram for the platinum microelectrode with no elec-



**Figure 5.** Complex plane plots for electrodeposited platinum films in PBS. The deposition potentials are indicated in each figure.

trodeposited platinum (Fig. 7a) shows the same general features as annealed polycrystalline platinum films with two well-defined hydrogen adsorption and desorption peaks, a double-layer charging region, an oxide formation plateau, and an oxide reduction peak.

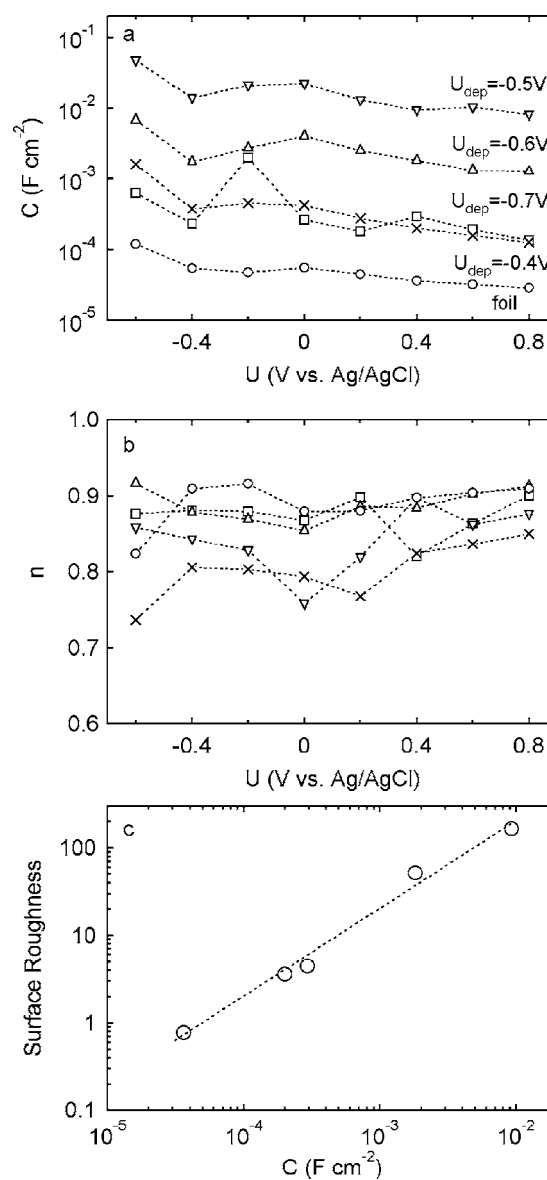


**Figure 6.** (a) The logarithm of the parallel capacitance vs potential for an annealed polycrystalline platinum foil and electrodeposited platinum thin films in PBS. (b) Exponent  $n$  vs potential. (c) Surface roughness vs the capacitance measured at 0.4 V. The surface roughness was determined from the hydrogen desorption charge in voltammograms in 50 mM  $\text{H}_2\text{SO}_4$  based on a monolayer desorption charge of  $210 \mu\text{C cm}^{-2}$ . ( $\square$ )  $U_{\text{dep}} = -0.5 \text{ V}$ , ( $\Delta$ )  $U_{\text{dep}} = -0.6 \text{ V}$ , ( $\square$ )  $U_{\text{dep}} = -0.7 \text{ V}$ , ( $\times$ )  $U_{\text{dep}} = -0.4 \text{ V}$ , ( $\circ$ ) foil.

The voltammograms for the electrodeposited microelectrodes, shown in Fig. 7b, have the same general features, although the currents are larger, especially for the films deposited at  $-0.5$  and  $-0.6 \text{ V}$ .

Figure 8 shows the surface roughness of the electrodeposited microelectrodes obtained from the hydrogen desorption charge. The roughness factor for the microelectrode deposited at  $-0.4 \text{ V}$  is about 4. In contrast, the roughness factor for the high-surface-area electrodes deposited at  $-0.5$  and  $-0.6 \text{ V}$  are more than an order of magnitude larger. The films deposited at more negative potentials have roughness factors in the range 10–15.

Charge injection experiments were performed on the electrodeposited platinum microelectrodes using a biphasic current pulse, as illustrated in Fig. 9. The charge needed to depolarize a cell is typically 5–500 nC, depending on the cell type, proximity to the cell,

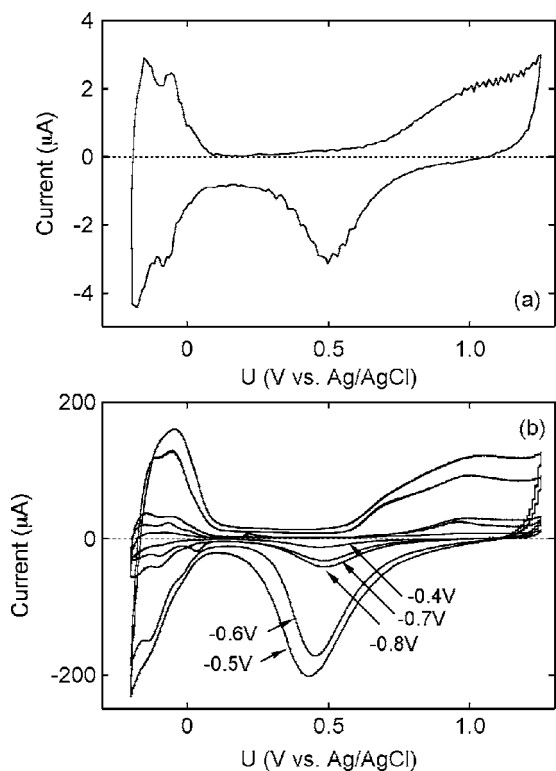


**Figure 7.** Current–voltage curves for (a) polycrystalline platinum microelectrode and (b) electrodeposited microelectrodes in 250 mM  $\text{H}_2\text{SO}_4$ , pH 1.8. The potential range was  $-0.2$  to  $-1.25$  V, and the scan rate was  $250 \text{ mV s}^{-1}$ . The deposition potentials are indicated in the figure.

and pulse duration.<sup>9,21</sup> The charge injected during each half-cycle in these experiments was  $200 \text{ nC}$  (corresponding to a geometric charge density of about  $7.1 \times 10^{-5} \text{ C cm}^2$ ).

Figure 9 shows the potential response (measured between the working and counter electrodes) to  $\pm 200 \mu\text{A}$  current pulses  $1 \text{ ms}$  in duration. The responses of all electrodes exhibit an initial, rapid change in potential followed by a longer period of more gradual potential displacement. On applying  $-200 \mu\text{A}$ , the initial potential decrease of about  $10 \text{ mV}$  corresponds to the IR drop in the system (about  $100 \Omega$ ). The microelectrode deposited at  $-0.4 \text{ V}$  exhibits a large potential excursion, decreasing to about  $-0.4 \text{ V}$  after  $1 \text{ ms}$ . In contrast, the high-surface-area films deposited at  $-0.5$  and  $-0.6 \text{ V}$  (Ag/AgCl) show relatively small potential excursions of less than

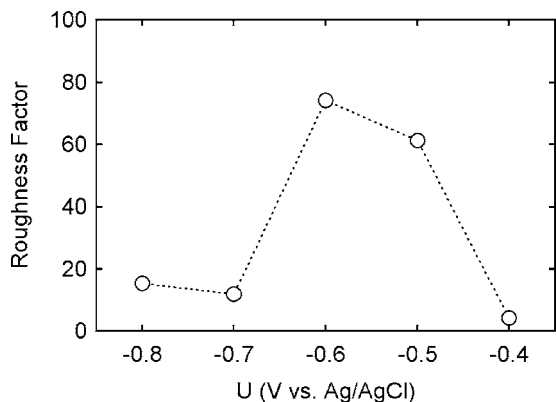


**Figure 8.** Surface roughness for electrodeposited platinum microelectrodes obtained from the hydrogen desorption charge in the potential range from  $-0.2$  to  $0.1 \text{ V}$  (assuming  $210 \mu\text{C cm}^{-2}$  for monolayer desorption).

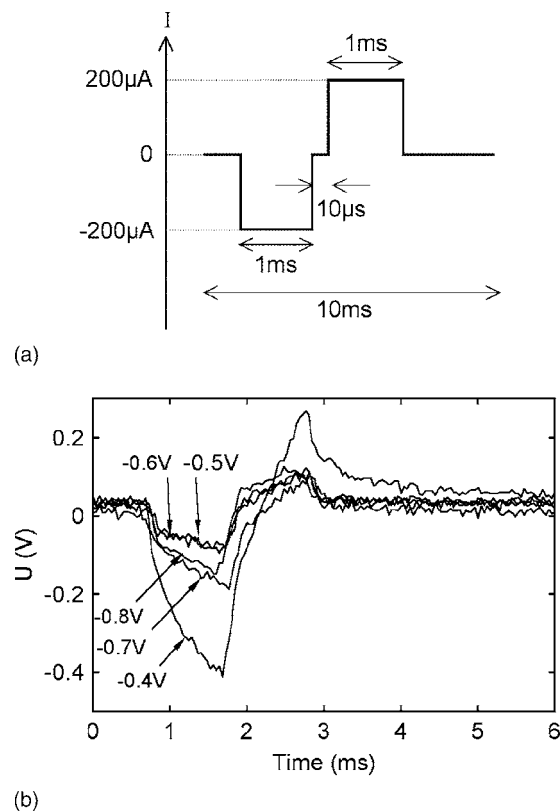


**Figure 9.** (a) Schematic illustration of the biphasic waveform. (b) Potential–time transients recorded for electrodeposited platinum microelectrodes.

$100 \text{ mV}$ . The films deposited at  $-0.7$  and  $-0.8 \text{ V}$  (Ag/AgCl) exhibit intermediate behavior. These results are consistent with the surface roughness values for the microelectrodes shown in Fig. 8. On switching the polarity of the current to  $+200 \mu\text{A}$  the potential of the microelectrode deposited at  $-0.4 \text{ V}$  (Ag/AgCl) increases to about  $0.25 \text{ V}$ . The other electrodes show much smaller potential excursions, increasing to about  $+0.1 \text{ V}$ .

In considering the performance of implantable electrodes, the two most important reactions to consider are hydrogen and oxygen evolution. The equilibrium potential for the hydrogen couple at this pH is  $U_{\text{eq}} = -0.644 \text{ V}$  (Ag/AgCl), and the current onset in the voltammogram at  $-0.84 \text{ V}$  (Ag/AgCl) corresponds to an overpotential of about  $200 \text{ mV}$ . The equilibrium potential for oxygen at this pH is  $U_{\text{eq}} = 0.579 \text{ V}$  (Ag/AgCl) and the current onset in the voltammograms at  $0.78 \text{ V}$  (Ag/AgCl) corresponds to an overpotential of about  $200 \text{ mV}$ . We should also consider the dissolution reaction for which the relevant equilibrium potential  $U_{\text{eq}}^{\circ}(\text{Pt}/\text{PtCl}_4^{2-}) = 0.558 \text{ V}$  (Ag/AgCl).

The open circuit potentials (OCPs) of the electrodeposited platinum microelectrodes during the current pulse experiments were in the range  $0.329$ – $0.352 \text{ V}$  (Ag/AgCl). Thus, the most negative potential for the electrodeposited microelectrodes in response to the  $-200 \mu\text{A}$  current pulse of about  $-0.4 \text{ V}$  corresponds to about  $-0.07 \text{ V}$  (Ag/AgCl), well above the equilibrium potential for hydrogen evolution. Similarly, the most positive potential in response to the  $200 \mu\text{A}$  current is about  $0.11$  or  $0.44 \text{ V}$  (Ag/AgCl) for the platinum electrodes except those deposited at  $-0.4 \text{ V}$  (Ag/AgCl). The electrodes deposited at  $-0.4 \text{ V}$  exhibit a potential of  $0.26$  or  $0.59 \text{ V}$  (Ag/AgCl), above the equilibrium potentials for oxygen evolution and dissolution.

Thus, the microelectrodes deposited at potentials between  $-0.5$  and  $-0.8 \text{ V}$  (Ag/AgCl) can deliver  $200 \text{ nC}$  of charge without evo-

lution of hydrogen or oxygen. As described above, the injected charge of 200 nC is much larger than typically needed to depolarize a cell, especially for electrodes in close proximity to the cell. Indeed, the high-surface-area films deposited at  $-0.5$  and  $-0.6$  V (Ag/AgCl) maintain a potential window of less than 200 mV during the biphasic cycle. These results suggest that stimulation can be safely achieved with much smaller microelectrodes by exploiting the high surface area associated with platinum deposited at  $-0.5$  to  $-0.6$  V (Ag/AgCl) in ammonium hexachloroplatinate solution at neutral pH.

In comparison, we note that the injection of 20 nC of charge in 0.5 mA pulses from high-surface-area electrodes (geometrical area =  $0.0043$  cm<sup>2</sup>) formed by cycling platinum at high rate for several hours resulted in voltage excursions of about  $\pm 0.5$  V.<sup>6</sup> The relatively poor performance of these electrodes appears to be associated with a very high ohmic resistance. In our experiments, 200 nC of charge was delivered in 0.2 mA pulses from electrodes with a geometrical area of  $0.0028$  cm<sup>2</sup>, resulting in a voltage excursion of  $\pm 0.1$  V.

Finally, we note that the microelectrodes were very robust. Microelectrodes deposited at  $-0.5$  and  $-0.6$  V were pulsed for more than  $10^5$  cycles with no obvious change in potential response or in impedance response under open-circuit conditions.

### Conclusions

The electrochemical response of platinum microelectrodes in PBS is strongly dependent on the morphology and microstructure. We show that electrodeposited platinum microelectrodes in PBS can inject 200 nC of charge in a 2 ms biphasic pulse with a potential window as small as 200 mV.

Johns Hopkins University assisted in meeting the publication costs of this article.

### References

1. P. Heiduschka and S. Thanos, *Prog. Neurobiol.*, **55**, 433 (1998).
2. K. W. Horsch and G. S. Dhillon, *Neuroprosthetics: Theory and Practice*, World Scientific, River Edge, NJ (2004).
3. W. F. Agnew and D. B. McCreery, *Neural Prostheses: Fundamental Studies*, Prentice Hall, Englewood Cliffs, NJ (1990).
4. L. S. Robblee and T. L. Rose, in *Neural Prostheses: Fundamental Studies*, W. F. Agnew and D. B. McCreery, Editors, pp. 26–66, Prentice Hall, New York (1990).
5. J. D. Weiland, D. J. Anderson, and M. S. Humayun, *IEEE Trans. Biomed. Eng.*, **49**, 1574 (2002).
6. M. Tykocinski, Y. Duan, B. Tabor, and R. S. Cowan, *Hear. Res.*, **159**, 53 (2001).
7. R. D. Meyer, S. F. Cogan, T. H. Nguyen, and R. D. Rauh, *IEEE Trans. Rehabil. Eng.*, **9**, 2 (2001).
8. J. J. Whalen, J. D. Weiland, and P. C. Searson, *J. Electrochem. Soc.*, **152**, C738 (2005).
9. M. Mahadevappa, J. D. Weiland, R. J. Greenberg, and M. S. Humayun, *IEEE Trans. Neural Syst. Rehabil. Eng.*, **13**, 201 (2005).
10. M. E. Baumgartner and C. J. Raub, *Platinum Met. Rev.*, **32**, 188 (1988).
11. C. A. Marrese, *Anal. Chem.*, **59**, 217 (1987).
12. W. Franks, W. Schenker, P. Schmutz, and A. Hierlemann, *IEEE Trans. Biomed. Eng.*, **52**, 1295 (2005).
13. A. E. Bolzan, A. M. C. Luna, A. Visintin, R. C. Salvarezza, and A. J. Arvia, *Electrochim. Acta*, **33**, 1743 (1988).
14. B. E. Conway, B. Barnett, H. Angersteinkozłowska, and B. V. Tilak, *J. Chem. Phys.*, **93**, 8361 (1990).
15. D. B. Hibbert, K. Weitzner, B. Tabor, and P. Carter, *Biomaterials*, **21**, 2177 (2000).
16. D. B. Hibbert, K. Weitzner, and P. Carter, *J. Electrochem. Soc.*, **148**, E1 (2001).
17. S. Mailley, M. Hyland, P. Mailley, J. A. McLaughlin, and E. T. McAdams, *Bioelectrochemistry*, **63**, 359 (2004).
18. J. R. Macdonald, *Impedance Spectroscopy: Emphasizing Solid Materials and Systems*, Wiley, New York (1987).
19. T. Pajkossy and D. M. Kolb, *Electrochim. Acta*, **46**, 3063 (2001).
20. W. G. Pell, A. Zolfaghari, and B. E. Conway, *J. Electroanal. Chem.*, **532**, 13 (2002).
21. D. B. McCreery, L. A. Bullara, and W. F. Agnew, *Exp. Neurol.*, **92**, 147 (1986).